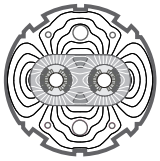

LHC Project Note 379

25 November 2005
Roderik.Bruce@cern.ch

BFPP losses and quench limit for LHC magnets

R. Bruce, S. Gilardoni, J.M. Jowett

Keywords: Quench, heavy-ion, magnet, luminosity, beam-loss

Summary

The performance of the LHC as a heavy ion (or proton) collider is limited by a number of physical processes in which beam ions are lost in superconducting magnets, depositing heat that could induce a quench. Bound Free Pair Production (BFPP) at the collision point is the most serious process for lead ion beams. This effect is studied quantitatively through simulations of the ion showers in a dipole magnet. An attempt is made to understand the level of energy deposition (from *any* kind of beam loss) that an LHC dipole magnet can withstand before it quenches. Finally the setup of the LHC beam loss monitor system was simulated in order to see if the present setup is suitable also for ions.

1 Introduction

Apart from protons, fully stripped $^{208}\mathrm{Pb}^{82+}$ ions with an energy of $2.76\,A\,\mathrm{TeV} = 0.574\,\mathrm{PeV}$ will also be collided in the LHC. When these ultra-relativistic ion beams collide in the LHC, many different physical processes take place. Apart from the hadronic nuclear interactions that will be the main objects of study by the experiments, there are also a number of other interactions that can influence and limit the performance of the collider in different ways. If the collisions are peripheral, that is, the lead ions do not collide head on but pass each other by with an impact parameter larger than the nuclear radius, the electromagnetic interactions dominate.

The electromagnetic processes with the largest cross section that can take place at the interaction points are Rutherford scattering and Free Pair Production [1]. These processes are very frequent (e.g., the cross-sections for free pair production run into the hundreds of kilo-barn) but rather harmless, since they do not significantly change the momentum of the ions [2]. There is however also a probability to produce an electron-positron pair with the electron created in a bound state of one of the nuclei. This process is called Bound Free Pair

Production (BFPP). Explicitly written, the reaction is:

$$^{208}\mathrm{Pb}^{82+} + {}^{208}\mathrm{Pb}^{82+} \xrightarrow{\gamma} {}^{208}\mathrm{Pb}^{82+} + {}^{208}\mathrm{Pb}^{81+} + \mathrm{e}^{+} \tag{1}$$

The absolute momentum change of the ions is negligible for this process also, but one of the ions changes its charge. For lead ions with $Z = 82$, this corresponds to a fractional change in magnetic rigidity of

$$\delta_{\mathrm{BFPP}} = \frac{1}{Z-1} = 0.012 \tag{2}$$

which is higher than the machine acceptance of $|\delta| < 0.006$ [2]. These ions, which have captured an extra electron, will form a secondary beam that will leave the wanted trajectory and be lost in a well defined location in the machine. This not only decreases luminosity over time but may also quench a magnet through localized heat deposition.

The severity of this effect depends on where in the LHC the ions end up but also on the probability for the BFPP reaction. Numerous references exist [3, 4, 5, 6], where the cross section for the BFPP process is determined both theoretically and experimentally. In [3], the cross section for BFPP is calculated using the plane wave Born approximation. Numerically, the resulting value for the total cross section for two colliding lead ions with $Z_1 = Z_2 = 82$ at an energy of 2.76 TeV/nucleon (the nominal ion energy in the LHC) is:

$$\sigma_{\mathrm{BFPP}} = 281\,\mathrm{barn} \tag{3}$$

This cross section refers to electron capture to one specific ion in the pair. The cross section for electron capture to either of the two ions involved is twice as large as the value given in equation (3). Today this is believed to be the best estimate available and is used in [1]. In [3] a comparison is made with other estimates and a fair agreement is found.

The value of this cross section can be compared with the total cross section for hadronic interactions between the colliding ion bunches. This cross section is $\sigma_{\mathrm{H}} = 8\,\mathrm{barn}$ according to Section 21.4 in [1].

In [1], the distribution of wrongly charged ions from IP2 on the beam screen was calculated with a special tracking package [7]. The ions form a spot, about 1 m long, in a dispersion suppressor dipole magnet about 400 m from the IP[1]. A picture of the beam envelope is shown in Figure 1. The BFPP reaction will take place at each IP where the ion beams collide.

In order to determine if the power deposition caused by BFPP imposes any danger of a magnet quench, Monte Carlo simulations of the particle shower in the magnet were first performed; these are described in Section 2. After that, in Section 3, an attempt is made to understand how the temperature changes inside the magnet due to this heat load and whether or not it will quench the magnet. These considerations are equally applicable to other kinds of beam loss, notably protons. Finally, the setup of the beam loss monitor system in the LHC ring was simulated. The present design is optimized for protons and in Section 4 new simulations were performed in order to determine if this setup is suitable also for ions.

[1] Slots 10R2 and 10L2

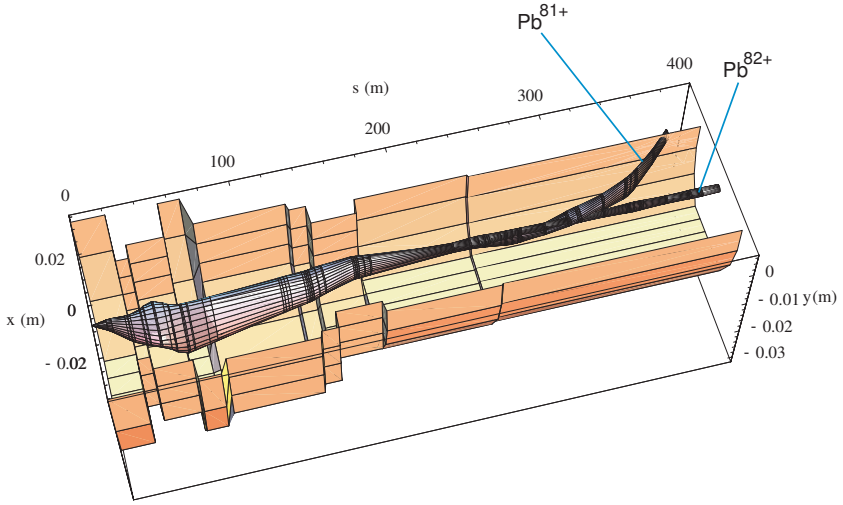

Figure 1: The traces of the primary beam and the secondary beam produced by BFPP through the beam pipe. The interaction point is at the left edge where the beam envelope is very small. To the right in the figure, almost 400 m from the interaction point, the main beam is going straight while the wrongly charged secondary beam leaves the trajectory and hits the beam screen. The figure is taken from [1].

2 Simulation of the shower in a LHC main dipole

2.1 Simulation setup

In order to determine the energy deposition caused by the lost ions, Monte Carlo simulations were performed with the program FLUKA [8, 9]. The full geometry of a LHC main dipole in three dimensions was implemented, based on a model from [10]. Some simplifications of the magnet geometry were made. The real dipole section is slightly bent but the angle covered by one magnet is for this purpose negligible, so the dipole was modelled as a straight cylinder. Some of the outer parts far from the regions of interest were simplified or completely left out. The coils themselves were approximated as made of copper instead of the real mixture of niobium, titanium and copper. The coils consist of 62.2% copper with an atomic weight of 63.55 u, 17.8% niobium with a weight of 92.91 u and 20% titanium with a weight of 47.87 u. So the average atomic weight of the coils is 65.64 u, very close to that of copper. Since the atomic weight is the most relevant parameter for the energy deposition, this approximation is very close to reality.

A transverse cross section of the real dipole and the computer model can be seen in Figure 2. The origin of the coordinate system was placed at the centre of one of the beampipes, at the beginning of the dipole with the z-axis pointing along the pipe in the direction of the beam.

The magnetic field in the coils has an influence on the secondary particle shower and thereby also on the deposited energy. It must therefore be included in the simulation with the correct magnitude outside the beampipe. This was achieved by linear interpolation of a field map from [11] that gave values of the true magnetic field in the dipole every 0.5 cm in the x-y-plane.

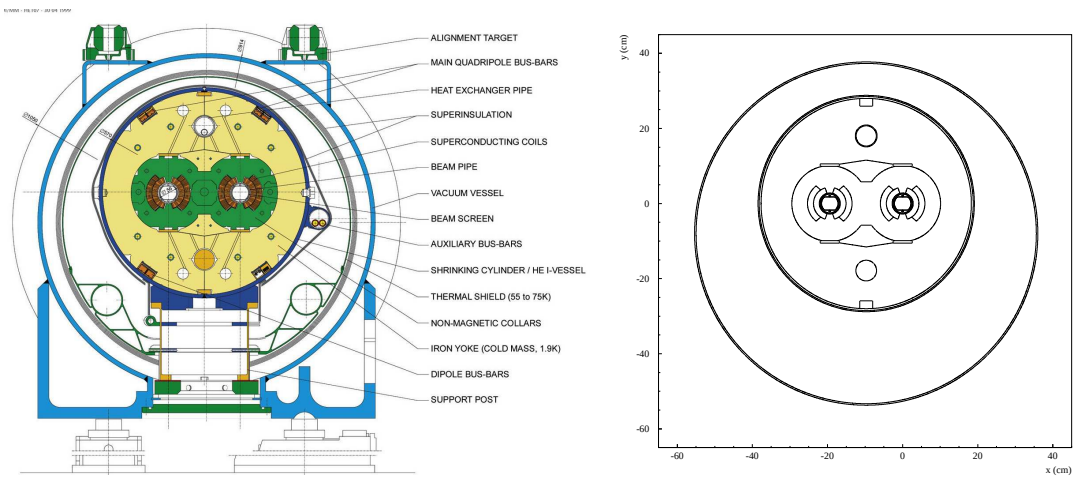

Figure 2: The transverse cross section of an LHC dipole magnet (left) and the FLUKA computer model (right).

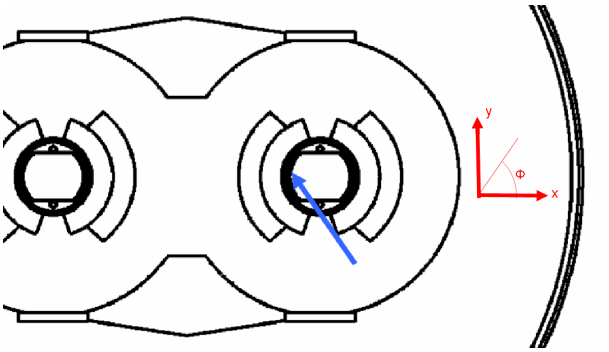

Figure 3: A schematic picture of how the beam hits the inside of the pipe.

The footprint of the impinging beam on the beam screen was modelled as a Gaussian distribution in momentum and position following [7] and Section 21.4 in [1]. In physical space it was normally distributed around $z = 130\,\text{cm}$ with a standard deviation of 55 cm longitudinally. In the x-y plane, the angle ϕ was sampled from a normal distribution with average $-\pi$ rad and standard deviation $\pi/30$ rad. The momentum of the ion beam was normally distributed around $2.76\,\text{TeV}/c$ per nucleon directed with a 0.5 mrad angle towards the beam screen. The standard deviation was 0.01 % in the $z-$direction and 2 % in x and y. A schematic picture of how the beam hits the beam screen is shown in Figure 3.

2.2 Scoring methods and results

During the simulation, the energy deposition per incident primary Pb^{81+} and volume was scored in a spatial mesh defined throughout the geometry of the dipole magnet. Once this energy deposition was known, the total power density from the lost beam was obtained through multiplication of the energy density per ion with the number of ions per time unit that undergo BFPP—that is, the cross section σ_{BFPP} for the reaction times the luminosity L. With the full design luminosity L from Section 21.4 in [1] and Eq. (3), the total power

Binning:	Old cylindrical	Medium cylindrical	Small cylindrical	Xsmall cylindrical	Cartesian
Δz[cm]	5	1	0.1	0.01	1
z_{min}[cm]	-4460	-4460	-4310	-4302	-4460
z_{max}[cm]	-3000	-3000	-4290	-4300	-3000
Δr[cm]	1.55	1.55	0.1	0.01	
r_{min}[cm]	2.8	2.8	2.8	2.8	
r_{max}[cm]	4.335	4.335	3.5	2.9	
$\Delta\phi$[rad]	$2\pi/88$	$2\pi/88$	$2\pi/176$	$2\pi/176$	
Inner arc [cm]	0.2	0.2	0.1	0.1	
Outer arc [cm]	0.310	0.310	0.125	0.104	
Δx[cm]					0.25
Δy[cm]					0.25

Table 1: The dimensions of the meshes used in the inner coil. The Δz, Δx, etc are the lengths of the cell in z- or x-direction. The inner arc is the inner length of the arc in the innermost cell, and the outer arc is the length of the outer arc in the outermost cell.

$P(\mathbf{r})$ deposited per volume at position $\mathbf{r}$ in the coils corresponds to an energy deposition $E(\mathbf{r})$ per volume and primary lead ion through:

$$P(\mathbf{r}) = E(\mathbf{r})\sigma_{\mathrm{BFPP}}L = E(\mathbf{r}) \times 2.81 \times 10^5 \mathrm{W/cm}^3 \tag{4}$$

The next problem was to determine the appropriate size of the cells in the mesh. The inhomogenous distribution of the secondary beam means that the power is not homogeneously distributed in the superconductors. If, for instance, one took the whole magnet as one cell, the value of the deposited energy per volume would be much lower than if one instead considered a very small cell around the place where the centre of the beam hits the coil. So with a smaller mesh the highest value of the deposited energy per volume is larger. Moreover, if the mesh is made finer and finer, the value of the maximum energy deposition will converge if the area of the beam is finite.

On the other hand, too fine a mesh will also result in troubles. Since only a limited number of primary particles are simulated and averaged over, there will be statistical fluctuations. So the distribution of the spots on the beam screen where an ion hits will not be smooth. The spots in the coils located exactly behind the points on the beam screen where an ion hits will therefore get a very high average energy deposition, while spots lying in between will get a lower average. If the mesh is made very fine, some cells will cover only these peaks where an ion hits, and these cells will therefore have a very high average value of the deposited energy. Also the fact that the minimum propagating zone for a quench in the LHC superconducting cables is of the order of 1 cm [12] implies that it is not necessary to use a very small mesh.

So what, then, is the best mesh to use, in which the cells are small enough to resolve the peak but large enough not to zoom in on the statistical fluctuations? The answer is hard to determine a priori, although some knowledge about the physical processes involved can give rise to an educated guess. If a steady state condition is considered, it turns out to be

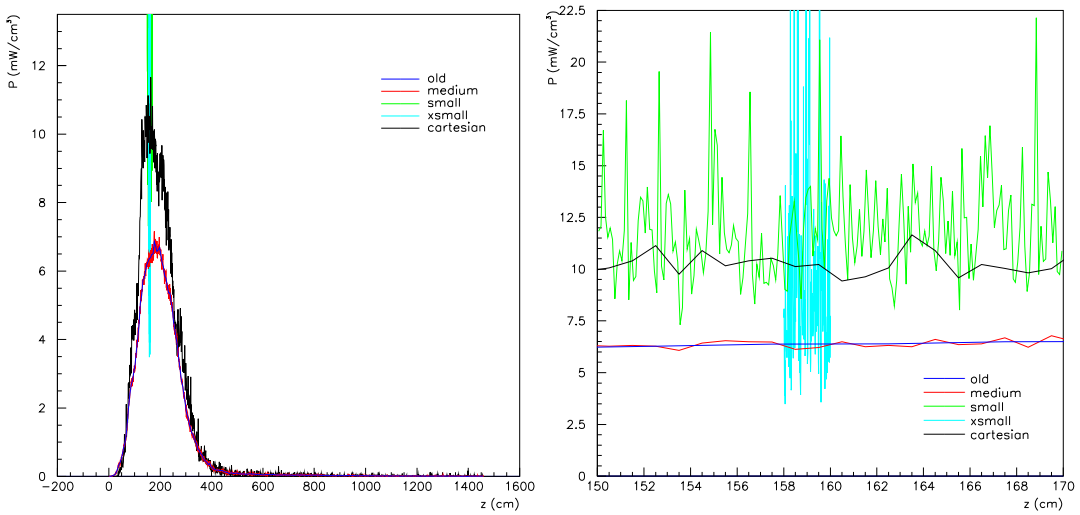

Figure 4: The power density for the *old*, *medium*, *small* and *xsmall* meshes plotted against z for $\phi = \pi$ rad and the smallest possible r (at the hot spot).

necessary to average the power over the radial dimension of the cable in order to compare the result with the experiments performed in [13]. This is explained further in Section 3.1. In the ϕ-direction, a superconducting cable can be well approximated as a single thermal body, while the heat transfer rate between different cables is low due to the cable insulation. Therefore the dimension of the thickness of a cable, around 2 mm according to table 7.1 in [1], is a suitable length of the arc in the cell. Longitudinally, a first estimate of a suitable cell length is 1/3 of a nuclear interaction length in copper, which is 15 cm according to [14]. This will capture a large part of the energy deposition originating from one primary lead ion inside one cell, thus considerably suppressing the effect of the statistical fluctuations without making the volume unnecessarily large. Another interesting longitudinal binning is a Δz of 15 cm, since this was the length of the plates used in [13].

When very short timescales are considered, the peak value of the energy deposition is needed. It is not obvious how to choose the mesh here. To explore the problem, one FLUKA run was made in which five different meshes in the inner coil were used simultaneously. Four of them used cylindrical coordinates with the z-axis in the centre of the beam pipe and in the direction of the beam, with the particles impinging at $\phi = \pi$ rad. The other mesh had Cartesian coordinates. The dimensions of the different binnings are given in Table 1. The *old* mesh is the one described above. The other meshes are finer in order to see how the maximum converges and the fluctuations come into play. The *old* and *medium* meshes were also used in the outer coil. Some 250 primary particles were transported in the simulation.

The results are plotted as power deposition per unit volume against z for a fixed r and ϕ for the various binnings in Figure 4. In Figure 5 the energy deposition scored with the medium binning is shown for the inner and outer coils. The black spot where the beam hits the beampipe is the hottest part and the place where the danger of a quench is greatest. In Figure 6 the energy deposition in a thin horizontal slice through the centre of the magnet is plotted.

As can be seen in Figure 4, the *old* and *medium* binnings are less dominated by oscillations

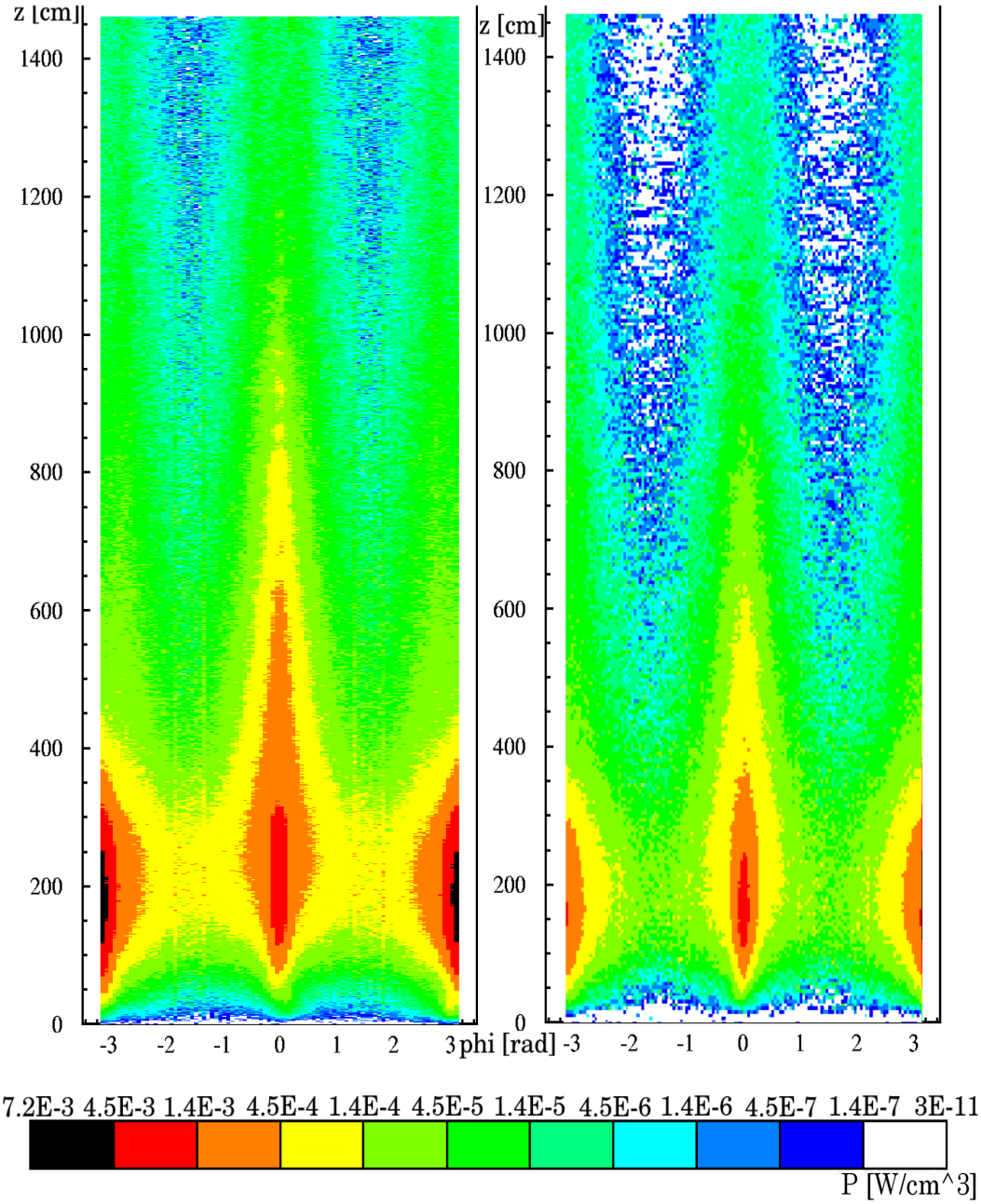

Figure 5: The energy deposition in the inner coil (left) and outer coil (right) scored with the medium mesh plotted with colour codes in the ϕ-z plane (only one bin was used in the radial direction). The primary impacts of the incident ions are normally distributed around $\phi = \pm\pi$ rad. The hot spot around $\phi = 0$ rad comes from the secondary shower caused by particles created on the other side of the beam pipe.

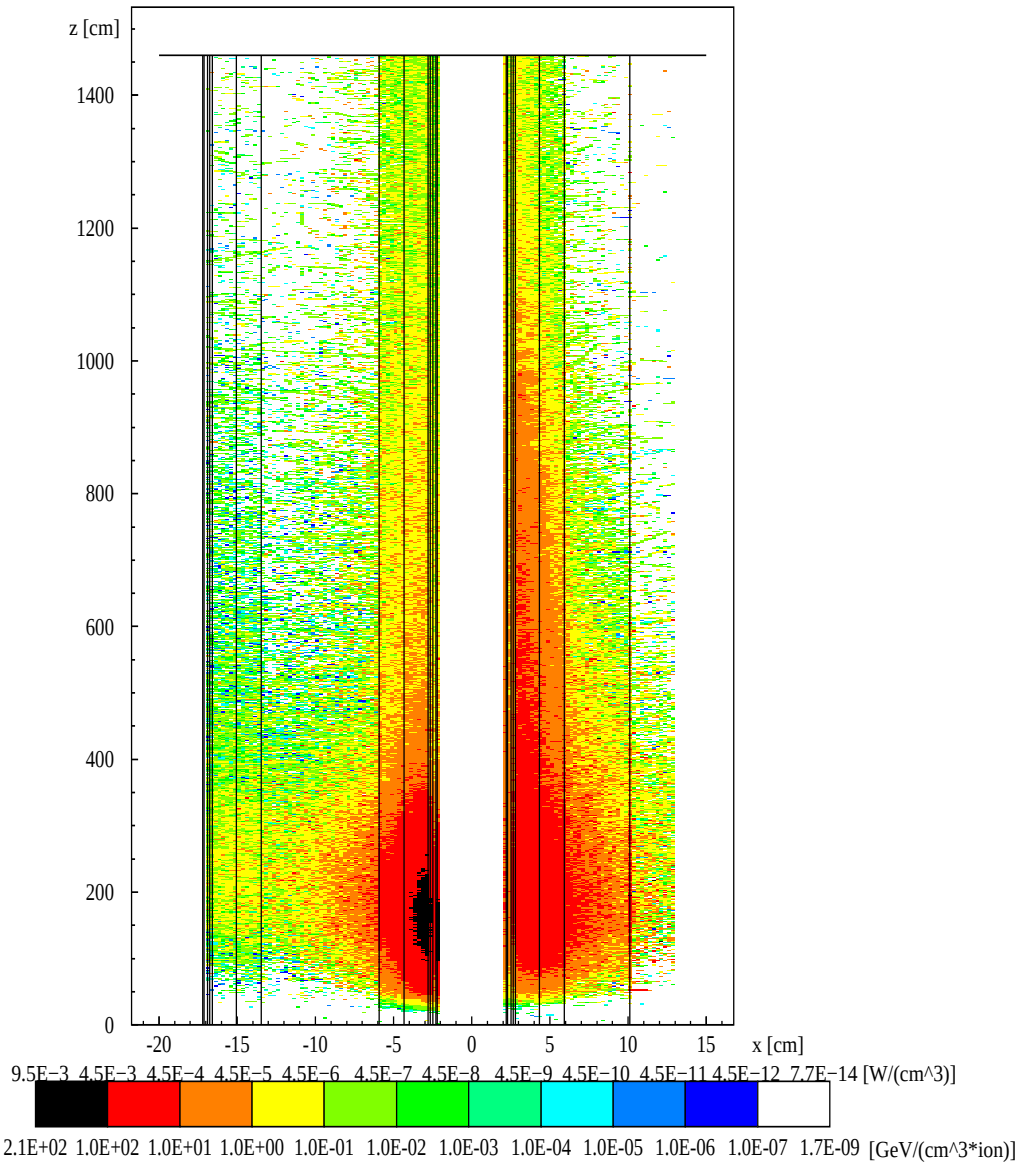

Figure 6: The energy deposition from BFPP in a thin horizontal slice around $y = 0$ scored with the *cartesian* mesh plotted with colour codes in a horizontal plane of width 0.25 cm around the vertical centre of the dipole. The white vertical stripe is the beam pipe where no energy is deposited, and the two stripes on each side are the coils. The black spot to the left is the hottest part where most of the ions hit the beam screen. The other beam pipe is to the left of the region shown.

Binning:	Old	Old 2	New 1	New 2	New 3
Δr(cm)	1.55	1.55	1.55/4	1.55/8	1.55/16
Δz(cm)	5	15	5	5	5

Table 2: The dimensions of the new meshes used. The other dimensions were the same as for the *old* mesh.

due to poor statistics than the *small* and the *xsmall* ones, so the maximum values of the *small* and the *xsmall* meshes should not be taken too literally. However, the average values of the *small* and *Cartesian* binnings are fluctuating around values higher than the average of the larger binnings. This is due to the binning in r, which raises the mean and which is not present in the *medium* and *old* mesh. So the higher averages give a warning that, if the binning in r is made finer, the maximum could grow, possibly without introducing large fluctuations.

Thus the conclusion is that the *old* mesh and the *medium* mesh have good longitudinal and azimuthal binnings for avoiding the spiky behaviour of the curve, but that a finer radial binning may raise the maximum. So for the steady state case, where no radial binning is needed, the *old* and the *medium* meshes are sufficient. However, for the transient case, it is necessary to obtain the maximum. Therefore another FLUKA run with three new meshes was performed. These meshes all have the same longitudinal and angular binning as the *old* mesh, but differ radially. The various radial binnings can be seen in Table 2. Also one mesh with the 15 cm longitudinal binning called *old 2* was used in order to compare directly with the results in [13], which will be described in Section 3.

The result can be seen in Figure 7. It is clear from this figure that the absolute maximum converges to 13.5 mW/cm^3 as the binning in r is made finer. For the steady state case, the *old*, *old 2* and *medium* binnings give very similar results. As maximum for the radial average both the *medium* and the *old* binnings have a maximum power density of 7.2 mW/cm^3. As might be expected, both maxima occur in the inner coil at the spot where the beam hits, as can be seen in Figure 5.

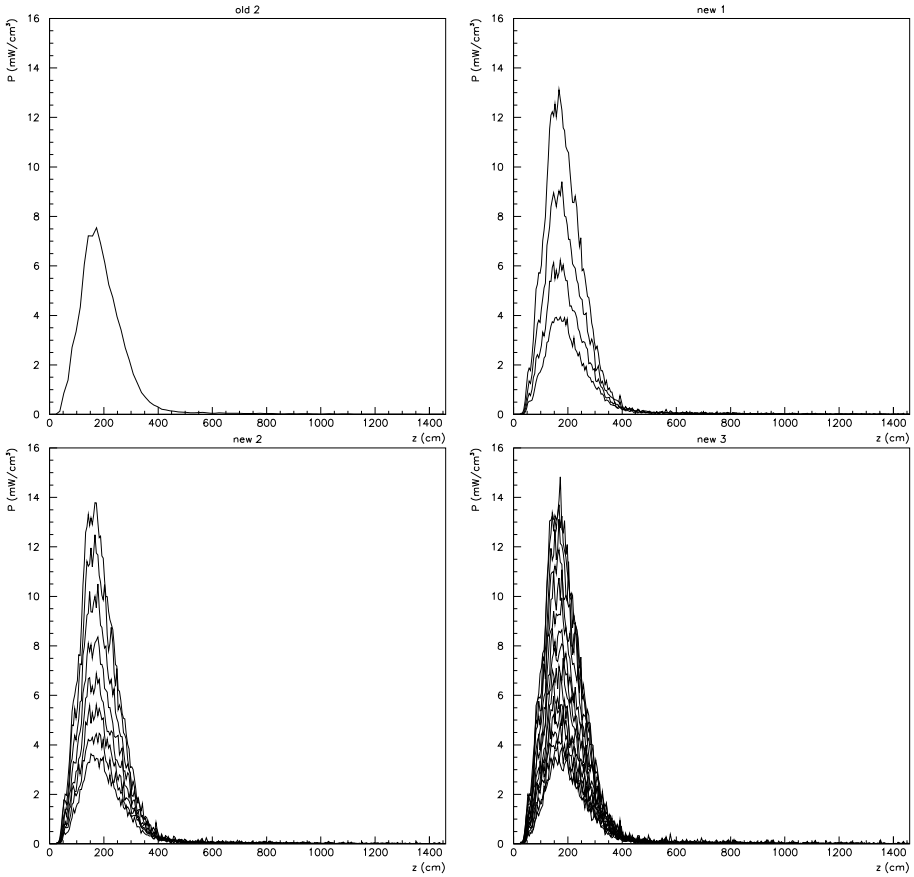

Figure 7: The energy deposition for the *old 2*, *new 1*, *new 2* and *new 3* meshes plotted against z for $\phi = \pi$ rad for all possible values of r. The highest curve is for the smallest r-value in each diagram. As the radial binning is made finer, the maximum power density converges to 13.5 mW/cm^3. The peak in the curve for the smallest r-value in the *new3* mesh is clearly a statistical fluctuation and therefore ignored.

3 Quench limit

In this section, an attempt is made to understand how the temperature rises in the superconducting LHC cables when some power is deposited. From that it is possible to draw conclusions about the maximum power that the cable can tolerate before it quenches. This is done in Section 3.1. After that, in Section 3.2, these results are compared with the results from Section 2 in order to determine if the dipoles will quench because of BFPP. In order to further investigate the probability of a quench, also the transient case, that is the first instants of time after the beam has been put into collision, is considered in Section 3.3.

3.1 Quench limit for the LHC main dipoles

In order to determine if a dipole magnet quenches or not due to the energy deposition from the BFPP, one has to calculate whether the temperature rise inside the superconductor is high enough to bring it over the critical surface in the space spanned by temperature, magnetic field and current density. From thermodynamics, the heat δQ per unit volume needed to cause a temperature rise dT is

$$\delta Q = C\, dT \tag{5}$$

if the material has a specific heat C, which is normally a function of temperature. $C(T)$ can be given as a fixed number for a specific body, or per weight or volume unit. In this report, C will have the dimension J/(cm^{3}K), meaning that the energy δQ will be given per unit volume in units of J/cm^3. On very short timescales, of the order of milliseconds, one can assume that no heat is transported away from the local point where it is deposited and that the temperature rise is a local process [15]. This can be useful in discussing transient losses or, perhaps, when analysing what happens during the first moments of operation after the LHC beams have been put into collision. Then Equation (5) can be integrated directly and one can set Q equal to the energy deposited by the lost ions during a given time interval:

$$Q = \int_{T_1}^{T_2} C\, dT \tag{6}$$

Here T_1 is the starting temperature, that is the temperature of the helium bath, and T_2 is the final temperature. The integral can be solved for T_2 which can then be compared with the critical temperature of the superconductor.

However, if steady state is considered, the situation is more complicated and the full heat flow has to be taken into account. The temperature profile $T(x,t)$ as a function of time and space can be obtained by solving the heat flow equation, which in one dimension reads [16]:

$$C(T)\frac{\partial T(x,t)}{\partial t} = \frac{\partial}{\partial x}\left(k\left(T(x,t)\right)\frac{\partial T(x,t)}{\partial x}\right) + P_{\text{loss}}(x) - P_{\text{He}}(T(x,t)) \tag{7}$$

Here $k(T(x,t))$ is the thermal conductivity of the cable, $P_{\text{loss}}(x)$ is the power input from the beam losses, which can be taken from Section 2, and $P_{\text{He}}(T(x,t))$ is the power taken away by the cooling system. If three dimensions are considered instead, the x-derivatives have to

be replaced by ∇ and appropriate scalar products. If steady state is considered, the time derivative on the left hand side can be set to zero.

The parameter that is difficult to determine in Equation (7) is $P_{\mathrm{He}}(T(x,t))$. Not only is there a large number of helium channels inside each cable, with the area between the helium and the conductors being very hard to calculate, but also the thermal behaviour of the helium is very complex. Several processes complicate any attempt to model the heat flow in the helium: The Kapitza resistance, which is the thermal boundary resistance when heat flows between a solid and liquid helium, the fact that the helium will start to boil next to the surface of the conductor, thus creating thin films of vapour next to the surface, and the counterflow process between fluid and superfluid helium [17]. It is also not well known a priori how the heat flows out of the cable, through the insulation.

However, there are other ways to make estimates of this heat transfer. In 1999, an experiment was performed by C. Meuris et al [13], in order to test the characteristics of different cable insulations. In these experiments, five plates made of stainless steel with a length of 15 cm were machined so as to resemble the geometry of the superconducting cable with the helium channels and insulated with different types of insulation. A temperature sensor was mounted in the middle of each plate. Then the plates were enclosed in a pressurized cryostat containing liquid helium, which was kept at a constant bath temperature.

In order to resemble the heating induced by the lost beam particles, a current was run through the plates, causing Joule heating. For a number of different types of insulation, the temperature difference between the central conductor in the stack and the helium bath was measured as a function of the power input. This can be seen in Figure 8, taken directly from [13]. These curves can also be inverted, in order to see the power transported away from the conductors as a function of the temperature difference, which one can use as the function $P_{\mathrm{He}}(T(x,t))$ in Equation (7).

Since only one temperature sensor was mounted in the middle of the cable, it is not meaningful to solve the heat flow equation radially. Although it is an approximation, the working hypothesis was chosen to be that the temperature is constant radially and one has to average the power input $P_{\mathrm{in}}(x)$ over the width of the cable. The azimuthal flow of heat between adjacent cables is small and not very well known in detail. Therefore a good first approximation of the problem is to solve the heat flow equation in one coordinate along the longitudinal direction. It is also worth noting that solving the full heat flow equation in three dimensions imposes severe numerical difficulties.

A rough first estimate of the temperature rise inside the conductors can also be taken directly from Figure 8 if one neglects the longitudinal heat flow. Then the expected temperature rise can be directly read in the diagram as a function of the power input from the particle losses. One can even put up an upper quench limit for the magnet — if the power deposition is lower than the power needed to raise the temperature to the critical one, neglecting the longitudinal heat flow, the magnet will not quench.

In fact, the LHC design report [1] states 4.5 mW/cm^3 as a limit for the maximum allowed power deposition inside the coils due to beam losses, with a reference to [13]. According to [1] it should have been concluded in [13] that a power input of 4 mW/cm^3 should cause a 1 K temperature rise, which through a linear extrapolation would indicate that an input of 4.5 mW/cm^3 causes a rise of 1.12 K. This is the allowed maximum rise due to beam losses if the temperature margin is 1.4 K as can also be seen from Table 7.3 in [1]. However, if one

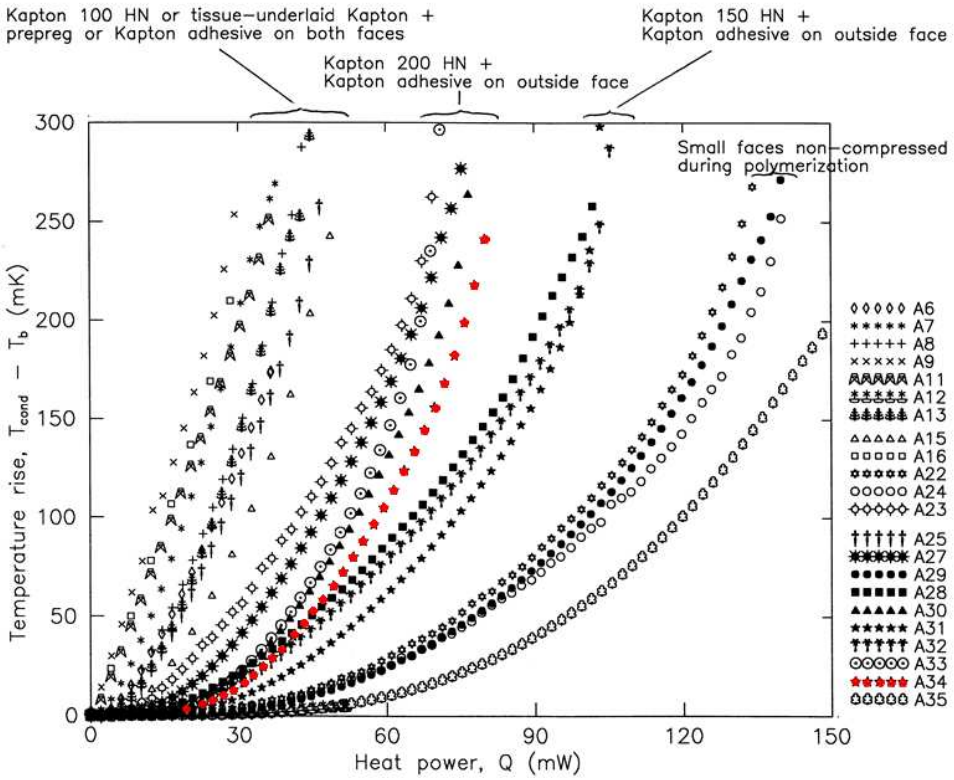

Figure 8: The temperature rise in the central conductor as a function of the power input for different cable insulations in the experiment described in [13]. The insulation that was actually chosen for the cables in the LHC dipoles is called A34. The power input is given as an absolute power—in order to get the power per volume one has to divide the scale with the volume 6.375 cm^3 that was used in the experiment. The figure is taken from [13].

examines the curve for the correct LHC insulation A34 shown in Figure 8, one can see from the highest point on the curve that an input of 79 mW in the reference plate (with a volume of 6.375 cm^3), which corresponds to 12.4 mW/cm^3, only causes the temperature to rise by 241 mK. This power is three times higher than the 4 mW/cm^3 that according to [1] should cause a rise of 1 K.

If one extrapolates this result beyond the range of the experiments with a fitted fourth degree polynomial, one arrives at temperature rise of 1.12 K for a power deposition of 19.3 mW/cm^3. This is more than four times higher than the limit proposed in the LHC design report [1]. However, this extrapolation is not very trustworthy, because the transition temperature at 2.167 K where helium goes from superfluid to fluid is passed. Normal fluid helium has a lower heat transfer coefficient, lower heat capacity and lower thermal conductivity than superfluid [17], meaning that the helium will take less heat away from the cable. Thus the real value of the power input should be lower than 19.3 mW/cm^3 meaning that the real quench limit derived from the experiment in [13] should be somewhere between 12.4 mW/cm^3 and 19.3 mW/cm^3.

A closer investigation showed that this discrepancy between [1] and [13] can be explained by the fact that before the experiments were done, it was postulated as a requirement on the machine performance that a power input of 4 mW/cm^3 should not cause a higher temperature rise in the conductor than 1 K. After that, the experiments in [13] were performed in order to confirm that this requirement was met. And these experiments showed that the thermal characteristics of the cable and insulation were actually even better, but the original number remained in the LHC Design Report for the sake of providing some extra safety margins [18].

There are however some uncertainties in the experimental results that could motivate these extra safety margins. First of all, the cooling conditions were not exactly the same as in the real dipole magnet. In the experiment, the cables were completely surrounded by a large helium bath of almost constant temperature. In the LHC cables, the flow of helium around the cables is limited and therefore less efficient than in the experiment. Also the shape of the cable is not exactly the same as the shape of the one in the experiment. The transverse cross section of the cable is not symmetrical: the end facing the beam pipe is thinner than the outer end. This was not the case in the experiment. How this would influence the thermal behaviour is not clear but it should not make a major difference.

On the other hand, a recent calculation of the critical temperature in the magnet by [11] shows that the magnet should be able to stand more than the 1.4 K mentioned above. The result of this calculation is shown in Figure 9. This should slightly increase the quench limit but it is very hard to say quantitatively by how much, since the curve in Figure 8 cannot be extrapolated due to the phase transition of helium. But, because of the worse heat transfer characteristics of helium above the phase transition described above, the gain is probably small.

Another thing worth noting is that the magnetic field in the coils decreases close to the ends of the magnet, thus increasing the quench margin. However, the helium cooling is not as efficient as in the centre due to the gluing of the end caps; this may reduce the number of channels for the helium flow. Taken all together, this would tend to make the quench limit lower. However, since the losses from BFPP hit at 1/3 of the magnet length, this issue is not a big concern in the context of BFPP.

The conclusion of the study of the quench limit is that there is a large uncertainty in

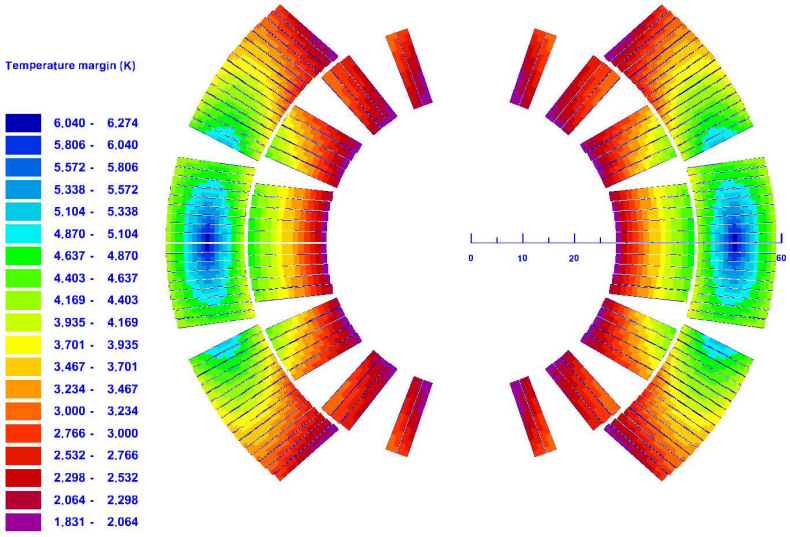

Figure 9: The temperature margin in K up to a quench in the coils of an LHC dipole magnet as calculated by [11].

the power taken out by the cooling system $P_{\mathrm{He}}(T(x,t))$. The best approximation available comes from [13]. But some uncertainties exist that could motivate extra safety margins. However it is very unlikely that the quench limit has to be decreased as far as the number given in [1]. In order not to have a too pessimistic limit, 10 mW/cm^3 was proposed by [18].

3.2 Conclusion for the steady state case

As was concluded in Section 3.1, the appropriate mesh for studying steady state losses has no radial binning. And as was shown in Section 2.2, the maximum for this type of mesh converges to 7.2 mW/cm^3. Comparing this value with the concluded new quench limit 10 mW/cm^3 from Section 3.1 directly, it is clear that the power deposition is not too high, although the margin is small.

A first rough estimate of the temperature profile caused by BFPP can be made directly with the data from Figure 8. If the longitudinal heat flow is neglected at first, each data point in the FLUKA output can be used as input to the correct function in this figure, which will return the temperature rise at that point. This has been done for the hottest cable in Figure 10. In the left part, the power deposition scored with the *old* mesh is shown, and in the right part the resulting temperature profile. As can be seen in the figure, the maximum temperature rise is only around 60 mK, which is an order of magnitude below the temperature margin of 1.12 K quoted in [1]. And so far no longitudinal heat flow has been taken into account.

A better estimate of the temperature profile is obtained through the solution of the full heat flow equation in steady state, that is Equation (7) with $\partial T/\partial t = 0$. The function $P_{loss}(z)$ is given by the FLUKA output and the function $P_{\mathrm{He}}(T)$ can be taken directly from the curve for insulation A34 in Figure 8.

However, when solving the one-dimensional equation, numerical difficulties arise because

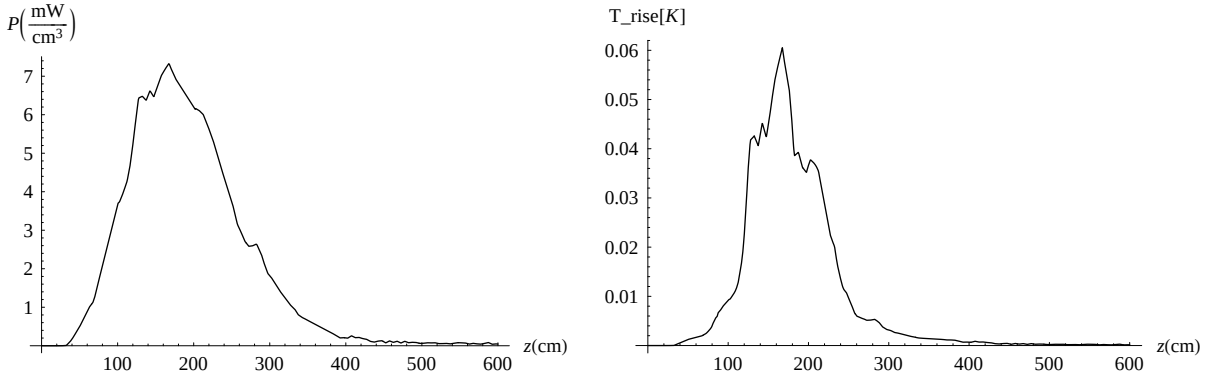

Figure 10: The power density in the hottest cable from the FLUKA simulation (left) and the resulting temperature profile (right) if no longitudinal heat conduction is taken into account.

of limited numerical precision. In order to demonstrate this, and also to investigate the qualitative effect of the heat transfer and see if it is worth writing a special numerical integrator for the heat flow equation, a very simplified model can be considered. The maximum power deposited in the cable is 7.2 mW/cm^3, but the shape of the curve for the power deposition as a function of z is rather complicated. In this oversimplified model the power deposition along the 1460 cm cable was approximated as a square function with the same integral of 1.22 W as the original FLUKA curve:

$$P_{\text{in}}(z) = \begin{cases} 0\,\text{mW/cm}^3, & 0 \le z/\text{cm} < 645 \\ 7.2\,\text{mW/cm}^3, & 645 \le z/\text{cm} < 815 \\ 0\,\text{mW/cm}^3, & 815 \le z/\text{cm} \le 1460 \end{cases} \tag{8}$$

The sharper distribution concentrates the heat more in the cable, which together with the fact that this distribution was placed in the middle of the cable makes the heat flow more important. In order to make the helium cooling less important it was modelled as a straight line

$$P_{\text{He}}(T) = P_0 T \tag{9}$$

with initially $P_0 = 50\text{mW/cm}^3\text{K}$ if T is the temperature rise and not the absolute temperature. Also the heat conductivity of the cable has to be taken into account. This is the weighted sum of the conductivities of copper and NbTi, with the copper to NbTi ratio 1.65 [15]. The heat conductivity for NbTi at temperature T is given by [19]:

$$k_{\text{NbTi}} = 7.5 \cdot 10^{-3} \cdot T^{1.85}\,\text{mW/(cm K)} \tag{10}$$

The heat conductivity for copper is not such a straight forward expression. At temperature

T and magnetic field B it is given by [19]:

$$
\begin{aligned}
k_{\mathrm{Cu}} &= \frac{2.44 \cdot 10^{-8} \cdot T}{\rho_{\mathrm{Cu}}(RRR, T, B)}\ \mathrm{mW/cm\,K} \\
\rho_{\mathrm{Cu}}(RRR, T, B) &= (1 + r)\left(\rho_i + \rho_0 + 0.4531\frac{\rho_i \rho_0}{\rho_i + \rho_0}\right) \\
\rho_0 &= 15.53 \cdot 10^{-9}/RRR \\
\rho_i &= \frac{1.171 \cdot 10^{-17} \cdot T^{4.49}}{1 + 4.498 \cdot 10^{-7} \cdot T^{3.35} \cdot \exp(-(50/T)^{6.428})} \\
\ln r &= -2.662 + 0.3168 \ln s + 0.6229(\ln s)^2 - 0.1839(\ln s)^2 + 0.01827(\ln s)^4 \\
s &= \frac{15.53 \cdot 10^{-9} \cdot B}{\rho_0 + \rho_i + 0.4531\frac{\rho_i \rho_0}{\rho_0 + \rho_i}}
\end{aligned}
\tag{11}
$$

Here ρ_{Cu} is the resistivity and RRR the residual resistivity ratio. This is a dimensionless parameter and a measure of the impurity of the specific material sample. For the copper in the LHC dipole cables, one has $RRR = 250$ [1]. In the simplified model, the heat conductivity was assumed to be constant. And in order to overestimate the influence of heat conduction compared with convection through helium this constant was chosen to be

$$k = 80\ \mathrm{mW/(cm\,K)}, \tag{12}$$

which is higher than all the real values in the actual temperature range and the real magnetic field in the coil, which is roughly between 1 T and 8 T.

Using equations 8, 9 and 12 together with the heat flow equation (7) with $\partial T/\partial t = 0$, the following differential equation is obtained:

$$k\frac{d^2T}{dz^2} - P_0 T = -P_{\mathrm{in}}(z) \tag{13}$$

It is worth noting that T in this equation is actually the temperature rise and not the absolute temperature because of the definition of P_{out}. The solution of Equation (13) is well known:

$$T(z) = C_i e^{\sqrt{\frac{P_0}{k}}z} + D_i e^{-\sqrt{\frac{P_0}{k}}z} + P_{\mathrm{in}}(z)/P_0 \tag{14}$$

Here C_i and D_i are integration constants that need to be determined through boundary conditions for the zones $i = 1, 2, 3$ determined by Equation 8. These were chosen so that T and dT/dz are continuous at $z = 645$cm and $z = 815$cm. Yet another way of increasing the importance of the heat flow is to require that the edges of the cable at $z = 0$ should be kept at the constant bath temperature $T = 0$. In reality it is not so simple: since the cables are wound in several turns, a more realistic boundary condition would be to require that the end temperature of one cable should equal the temperature in the beginning of the next cable on the other side of the beam pipe and so on, which requires that the heat equation is solved in all cables. This is not done in this simplified model.

The above mentioned boundary conditions give in total six equations that allow the integration constants to be determined numerically. However, when attempting to solve the

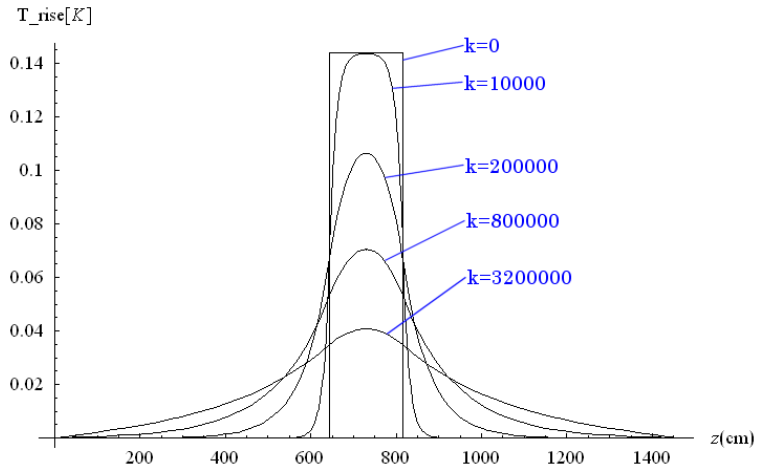

Figure 11: The temperature rise in the cable for different values of the thermal conductivity k[mW/(cm K)] calculated with the simplified model of the energy deposition and transfer.

system of equations with the initially proposed $k = 80\,\mathrm{mW/(cm\,K)}$ and $P_0 = 50\,\mathrm{mW/(cm^3 K)}$ numerical difficulties arise because of limited precision. This is due to the fact that, for these values, the resulting temperature profile is very similar to the profile one would reach without any heat flow—that is, the solution of Equation (13) if $k = 0$. As can be seen by inspection, this profile is a square wave with height $7.2/P_0 = 0.144$ K.

If one gradually increases k the heat flow slowly becomes important and starts influencing the shape of the temperature profile. This is shown in Figure 11, where the solution to Equation (13) is shown for several values of k. As can be seen in the figure, the heat conduction does not lower the maximum temperature in the cable significantly until k becomes very large. For $k = 200000\,\mathrm{mW/cm\,K}$ the maximum temperature in the cable has decreased by roughly 20%. Such large values of k are totally unrealistic, even if the temperature varies and the magnetic field changes. One should also bear in mind that the heat conduction was consequently overestimated and the heat transported away by the helium underestimated in the rough approximations in this very simplified model. Therefore it can be concluded that the longitudinal heat conduction is negligible as a source of heat removal when compared to the convection through the helium. It is a very good approximation to simply solve the equation $P_{\mathrm{He}}(T) = P_{\mathrm{in}}(z)$, which was done in Figure 10, and it is not necessary to solve the full heat flow equation. Here the maximum temperature rise in the hottest cable is 60 mK and taking into account the heat conduction along the cable does not change this value significantly.

The uncertainty lies instead in the function $P_{\mathrm{He}}(T)$ which is not well known but where the best existing estimate is given by [13] as explained in Section 3.1. Although some extra safety margins should be taken into account, it is however unlikely that the actual temperature rise is an order of magnitude higher. Thus it can be concluded that the risk of quenching the magnet with losses from BFPP in steady state is small.

However, another uncertainty, which was neglected so far, is that the power deposition of 7.2 mW/cm^3 calculated in Section 2.2 has an error bar which is very difficult to estimate. Because of numerical errors, limited statistics, possible limitations in the physics models used

and approximations of these models, this number may have a large uncertainty. FLUKA specialists suggest a safety margin of a factor two. This would imply a maximum power density of 14.4 mW/cm^3, which when used as input to the curve in Figure 8 lies outside the range of input values, meaning that extrapolation must be used and that the lambda point for helium at 2.167 K is passed. The total effect could be that the final temperature is higher than the critical one. A power density of 14.4 mW/cm^3 is also above the limit suggested by [18].

Yet another uncertainty factor lies in the radial averaging of the power input, which is necessary in order to compare with the experiments done in [13]. If instead the maximum power deposition of 13.5 mW/cm^3 is taken, and one also takes into account the safety margin of a factor two, it is clear that the magnet is probably over the quench limit.

So although a magnet quench due to BFPP is not likely to occur, it is impossible to exclude one due to the uncertainties in the quench limit and the simulation result itself. So far it has also been assumed that only the BFPP process causes ion losses at this particular spot. If other physical processes cause more power to be deposited in the coils, the danger of a possible quench increases.

3.3 BFPP Energy deposition on short timescales

In this section the danger of a quench is further evaluated through looking at BFPP on a very short timescale and considering what happens the first instants of time after the beam has been put into collision. Since it takes a certain time for the heat to migrate out of the cable and be conducted away by the helium, one can choose a timescale so short that all deposited heat stays within the cable so that the flow of heat can be neglected. Thus this consideration does not involve a steady state limit and the uncertain function $P_{He}(T)$. The time constants for the heat flow in the cable is compared with the time it takes for the cable to quench under these circumstances, given by Equations (19) and (21), and it is concluded that there is no danger of a quench on short time scales. If a quench would occur already here, it would be certain to happen also in steady state, which would falsify the calculations in previous section. But instead the result found in this section is consistent with the steady state calculation, although it can not validate it.

A similar calculation has already been performed for homogenous losses of protons [15], and this section will follow this calculation in broad outline but with some appropriate modifications and also improvements. A pessimistic approximation will be considered, where the luminosity goes from zero to the nominal value like a step function.

In order to understand whether or not a magnet quenches on a short time scale, one must calculate the temperature rise caused by the energy deposition and then compare it with the minimal temperature rise that brings the superconductor outside the critical surface at the present magnetic field and current. A map of this temperature margin T_{marg} in the coils has been computed for the nominal magnetic field and current by [11] and is shown in Figure 9.

One can note that the minimum temperature margin in this map is 1.8 K. In Table 7.3 in the LHC design report [1], a value of 1.4 K is given. This discrepancy is due to some recent changes in the design of the coils. In Table 7.3 in [1] some extra terms that decrease the temperature margin are listed. The measurement precision, dissipation and ramping losses mentioned there, decrease the margin by a total 0.34 K, which had therefore to be

subtracted from every point in the temperature margin map given by [11].

The amount of heat required to raise the temperature in the cable by a certain value can be calculated using Equation (6). In this case, the wires are almost free to expand locally since they are surrounded by liquid helium. Thus for wires immersed in liquid helium the specific heat at constant pressure, C_P, should be used. However, for a limited low temperature range in metals, $C_V \approx C_P$ [15], and the calculations become significantly simplified if instead C_V is used. Therefore C_V will be used throughout the calculations. The energy needed to raise the temperature in the superconductor from the temperature of the helium bath $T_{\text{bath}} = 1.9$ K to the temperature at the critical surface $T_{\text{bath}} + T_{\text{marg}}$ is:

$$Q = \int_{T_{\text{bath}}}^{T_{\text{bath}}+T_{\text{marg}}} C_V \, dT \tag{15}$$

The total specific heat of the coil is a weighted sum of the specific heat for each material it consists of, which is copper in 56.6% of the volume and NbTi in 35.4%. The remaining 8% of the volume is taken up by superfluid helium and insulation. Following [15], the insulation has a specific heat close to that of NbTi and a very small relative volume. Therefore it contributes very little to the total heat reserve and can therefore be neglected in this estimation.

The helium on the other hand contributes substantially to absorb the added heat—in this temperature range the specific heat of helium is orders of magnitude larger than that of NbTi, meaning it has to be taken into account. However, if very short timescales

$$t \ll 8 \times 10^{-3}\text{s} \tag{16}$$

are considered, as pointed out in [15], the heat does not have enough time to spread to the helium, since the flux of heat from the wire to the helium is limited. Thus, considering for instance the very first 100 μs, a timescale proposed by [20] which fulfils the restriction (16), the influence of the helium can be neglected.

Therefore two different timescales can be considered: first the 100 μs scale, where the helium does not contribute, and then the 8 ms scale, where the helium contributes but is not flowing. This corresponds to the cases a) and c) mentioned in [15].

3.3.1 Calculation without helium

Following [15], the specific heat of copper can be parametrized as

$$C_{V,Cu} = 9.686 \cdot 10^{-2} \cdot T + 6.684 \cdot 10^{-3} \cdot T^3 \ \ [\text{mJ}/(\text{cm}^3\,\text{K})] \tag{17}$$

and the specific heat of NbTi as

$$C_{V,NbTi} = 0.87 \cdot \frac{B}{B_{c2(0)}} \cdot T + 4.464 \cdot 10^{-2} \cdot T^3 \ \ [\text{mJ}/(\text{cm}^3\,\text{K})]. \tag{18}$$

Here B is the magnetic field and $B_{c2(0)} = 14$ T is the second critical field at $T = 0$. The total specific heat is then obtained by weighting C_V for Cu and for NbTi according to their relative volume fractions. Thus, with a working temperature of $T_{\text{bath}} = 1.9$ K an energy margin — that is the maximum energy per volume that can be added before the magnet quenches —

was calculated for every point on the temperature margin map with Equation (15). The minimum energy margin in the whole magnet was found to be 1.636 mJ/cm^3.

Now this margin has to be compared with the energy deposited by the lost ions. When considering a very short timescale, as stated in [15], the heat does not have sufficient time to migrate radially through the wire. This means that the correct value of the energy deposition to compare with is the very peak of the energy deposition as a function of radius at the hottest longitudinal coordinate, and not the radial average. According to Section 2.2, this value converges to 13.5 mW/cm^3. If this power is deposited in the coil during 100 μs, $1.35{\cdot}10^{-6}$ J/cm^3 is deposited in the hottest part of the magnet. This is three orders of magnitudes below the lowest energy margin. Thus it can be concluded that there is no risk of the heat deposition from BFPP quenching the magnets on the 100 μs timescale.

Indeed, even if the high heat capacity of the helium is not taken into account, and it is supposed that the highest energy density is deposited in the weakest part of the coil, the wire itself could stand this power for

$$\frac{1.636\,\mathrm{mJ/cm^3}}{13.5\,\mathrm{mW/cm^3}} = 0.12\,s \tag{19}$$

which gives enough time to dump the beam.

3.3.2 Calculation with helium

If one considers timescales long enough to allow heat to flow from the wire to the helium, but not long enough to let the heat be transported away by the helium flow, then the specific heat of the helium has also to be taken into account. The specific heat of liquid helium is a complicated function of the temperature. In [15] the integration was performed using tabulated data for C_P in the approximation that the density was constant. In this report a different approach was used. The specific heat was instead calculated with the software HEPAK 3.4 [21] to achieve higher accuracy.

For superfluid and fluid helium, C_V and C_P are qualitatively different, so the choice really matters and is not obvious. Although the cables are under high pressure inside the cryostat, the superfluid helium is at atmospheric pressure, since it can flow without resistance through the microscopic channels. Thus the starting point of the helium in the $P-V$ plane is at 1.9 K and approximately 1 atm before the heat deposition. The density of helium at this pressure and temperature is 0.147 g/cm^3 [15]. In Figure 12, C_V and C_P are shown as a functions of temperature at constant density or pressure. Both curves were calculated using HEPAK up to 9 K. It is worth noting, that in the C_V curve there is only one phase transition, between fluid and superfluid, whereas there are two transitions in the C_P curve. If the pressure is kept constant the transition to gas can also be seen. The phase transitions are the peaks in the diagrams: when the curve is integrated over a peak, the integral has a large value corresponding to the energy needed for the transition.

For a correct choice of integration path in the $P - V$ plane, the underlying physical processes have to be investigated in more detail. The cable is surrounded by an insulation which can stand some pressure but, if the pressure becomes too high, helium will evaporate out through the insulation [22]. A fair model would thus start the integration at constant volume but then, at the maximum pressure P_c that the cable insulation can stand, switch

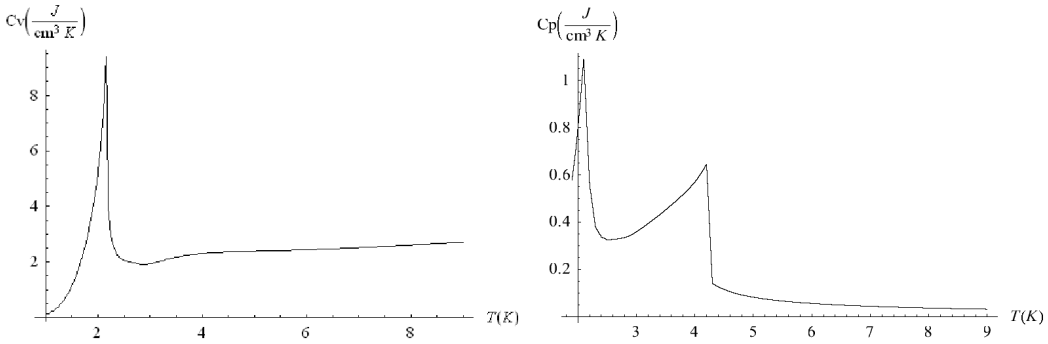

Figure 12: The specific heat C_V [J/(cm^3 K)] at constant density 0.147 g/cm^3 as a function of temperature [K] (left) and C_P [J/(cm^3 K)] at constant pressure 1 atm as a function of temperature [K] (right).

to an integration with constant pressure. If the temperature of the helium is $T(P_c)$ at this critical pressure, the integration of the specific heat of the helium becomes

$$\int_{T_{\text{bath}}}^{T_{\text{bath}}+T_{\text{marg}}} C_{He}\, dT = \int_{T_{\text{bath}}}^{T(P_c)} C_{V,He}\, dT + \int_{T(P_c)}^{T_{\text{bath}}+T_{\text{marg}}} C_{P,He}\, dT. \tag{20}$$

The value of P_c is not known and is very hard to estimate. The only hints known are observations in some experiments that thin films of helium actually start to boil close to the cable surface at quite low temperatures well included on the temperature axis in the shown diagrams [22]. This means that the critical pressure is well below the final pressure at 9 K in the C_V diagram, which according to the HEPAK calculation is 34 atm. It seems plausible that the cable could not hold this pressure inside.

In [15], the specific heat for helium was integrated from the bath temperature at 1.9 K to three temperatures: 2.168 K (the lambda point), 2.8 K and 9 K. In order to compare with these results, the specific heat for helium was integrated between the same points for several different cases: The extreme cases with only C_V or only C_P all the way, and several cases starting with C_V, and then when a critical pressure is reached, switching to C_P. The C_P integration has to start at the pressure and temperature where the C_V integration stopped. Thus a different C_P had to be calculated for each critical pressure. The values of C_V and C_P in units of J/(K cm^3) were calculated every 0.1 K from 1.9 K to 9 K using HEPAK and then linearly interpolated and integrated in Mathematica© [23]. The achieved values are given in Table 3 together with the reference values from [15].

The highest energies are obtained for critical pressures between 6 and 10 atm. As can be seen in Table 3, the integrated energies do not differ substantially at the lower integration boundaries depending on whether C_V or C_P is chosen. This is not the case for the integral to 9 K. Especially worth noting is the large value that was obtained in [15]. Regardless of how the critical pressure is chosen (the true value is not known as pointed out above), it is not possible to get a value as high as this using the HEPAK data. The discrepancy comes from the fact that a less accurate method was used in [15] due to lack of data. The integral up to 9 K comes in to play when looking at quench limits for the injection energy (450 GeV

P_c [atm]	Integral to 2.167 K	Integral to 2.8 K	Integral to 9 K
1	0.22	0.46	1.40
2	0.22	0.44	2.41
5	0.22	0.44	3.96
6.25	0.22	0.44	4.07
7.5	0.22	0.44	4.09
8.125	0.22	0.44	4.07
8.75	0.22	0.44	4.04
10	0.22	0.44	3.97
20	0.22	0.44	3.31
∞	0.22	0.44	2.67
Report 44 [15]	0.23	0.58	6.3

Table 3: The energy values obtained by integrating the specific heat as shown in Equation (20) up to three different temperatures. P_c is the pressure where the helium is assumed to start leak out through the cable insulation. At a critical pressure of 1 atm, C_P is used through the whole integration, and at a critical pressure of ∞ only C_V is used. The last line gives the values calculated in [15].

for protons), and the results above thus imply that the magnet will quench more easily than was earlier thought for this type of loss. Depending on the true value of the critical pressure, the energy that the helium can absorb should be decreased by at least a factor 1.5. In reality it may also well be the case that the process follows a different path in the $P - V$ plane, where none of these variables is constant. An investigation of this case is however beyond the scope of this text.

For the present problem with BFPP, it is not necessary to know the exact value of the critical pressure, and the lower temperature range, where the results are consistent, is the one of interest. In order to have safety margins, the most pessimistic case can be chosen, which is the case where C_P is integrated all the way. Physically, this would mean that the helium would start to leak out through the cable insulation as soon as it is heated, which is not the case in reality. However, choosing this integration path gives a pessimistic estimation.

So using Equation (6) and C_P for helium added with the appropriate weight in the heat capacity of the cable, an energy margin was once again calculated for every point in the coils. It was found that the minimum energy margin in the magnet was 34.9 mJ/cm^3. When considering this slightly larger timescale, the relevant value of the power deposition is not the peak value, but the radial average, since the heat has sufficient time to migrate radially in the cable [15]. This is, as mentioned earlier, 7.2 mW/cm^3 in the hottest part of the coil. Thus, during 8 ms, the energy density deposited in the cable is 0.0576 mJ/cm^3. This is again orders of magnitude below the quench limit, so there is no risk quenching the magnet on this timescale either. So, even if the maximum energy density was deposited at the weakest spot in the magnet, it would still take

$$\frac{34.9\,\mathrm{mJ/cm^3}}{7.2\,\mathrm{mW/cm^3}} = 4.85\ s. \tag{21}$$

before the magnet would quench.

The conclusion that can be drawn is that the magnet will not quench due to BFPP before the cooling system comes into play. This is consistent with the result for the steady state case. Since it will take seconds before enough heat to induce a quench is accumulated even without helium flow, it will take much more time when this cooling is present. So if the magnet were to quench in steady state after all, it would be a slow process where more and more heat is accumulated in the magnet over time, provided that no other processes increase the heat deposition.

4 The beam loss monitor system

In order to protect the magnets from quenches caused by beam losses, that in the worst case could even damage them, a beam loss monitor system will be installed around the LHC [24, 25]. The system will consist of small ionization chambers that will be placed just outside the cryostat. These beam loss monitors (BLMs) will detect secondary particles from the showers induced by beam losses. The correlation between the signal in a BLM and the energy deposited in the magnet coils has been determined for protons through simulations [24]. If the signal corresponds to a too high energy deposition, the beam is extracted and dumped.

For lead ions however, the correspondence between the signal in the BLM and the energy deposition in the magnet is different. Because of the high electromagnetic cross sections, the ions deposit more energy per volume before the nuclear breakup. This could mean that the same amount of detected shower particles outside the cryostat corresponds to a higher energy density in the coils in the case of ions. In order to investigate this problem more closely, FLUKA simulations were performed to determine whether the present design, optimized for protons, also could be suitable for lead ions.

4.1 Simulation setup

The most straight-forward way of finding out if the setup for protons is suitable also for ions is to simulate the impact of both ion and proton beams in an LHC magnet and then compare the ratio between energy deposition in the coil and in a detector outside the cryostat for both particle types. The output signal is approximately directly proportional to the energy deposition in the BLM. The particles hitting the BLMs have a low energy, so the dominating source of energy loss in the gas is ionization, which in turn gives rise to the output signal. The model of the BLM does not need to be exact in this case, since the ratio and not the absolute number is the quantity of interest. In [25] the BLMs were modelled as thin rectangular chambers with iron walls filled with N_2. This is not the real shape, but this approximation is good enough for present purposes.

For convenience, the dipole model from the simulation of the BFPP shower was used again, with the modelled BLMs added outside the cryostat. The transverse cross section of the computer model is shown in Figure 13. Also the same magnetic field map was used. At first one might suspect that this fieldmap, which only covers the cold mass, is not precise enough, since the particles giving rise to the signal in the BLMs have to traverse the void

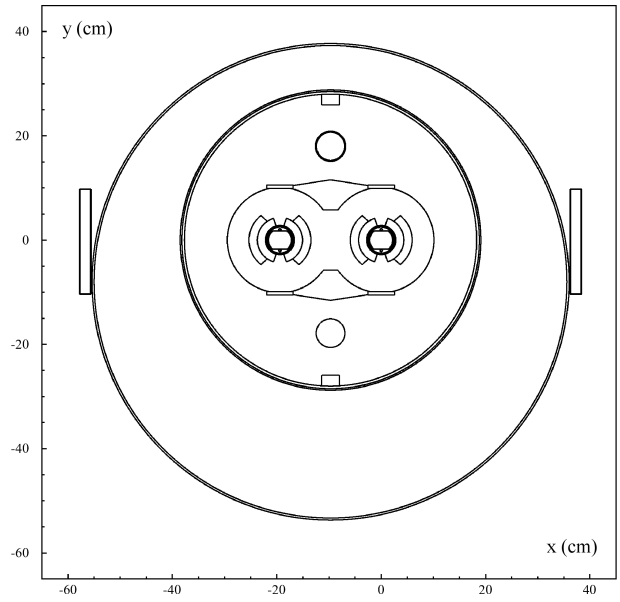

Figure 13: The transverse cross section of the computer model of the dipole with the BLMs.

outside the cold mass, where there is a weak magnetic field, on the order of μT. Therefore a larger magnetic fieldmap extending 30 cm outside the cryostat was obtained from [11]. However, two otherwise identical FLUKA simulations showed that this difference is negligible. Therefore the smaller fieldmap was used in the following simulations, because the tracking in FLUKA is faster and more accurate in regions without magnetic field.

So different simulations had to be performed, both with 7 TeV protons and 2.76 TeV/nucleon lead ions in the same geometry. The beam used was a pencil like beam impinging at z=0 in the beginning of the magnet at an azimuthal angle of $-\pi$ and with an incident angle of 25 mrad. The pencil beam, used as a δ-function, can symbolize any beam loss.

4.2 Results

In Figure 14 the results from all FLUKA simulations are shown. The curves have quite similar shapes. This becomes even more clear when regarding Figure 14 (right), where the function

$$f(z) = \frac{E_{\text{ions,coil}}(z)/E_{\text{ions,BLM}}(z)}{E_{\text{protons,coil}}(z)/E_{\text{protons,BLM}}(z)} \tag{22}$$

is plotted. Here E is the energy deposition per volume and primary particle. As can be seen in the figure, this curve is fluctuating around 1 or even below, meaning that the ratio between energy deposited in the coil and in the BLMs is approximately the same for ions and protons. The peak in the beginning of the curve is clearly a statistical fluctuation. It is also not as important as one might think, since Figure 14 shows that the absolute maximum for both curves, which is the critical part for determining quenching, is located at $z = 25\,\text{cm}$.

Physically, one might expect a larger difference between the curves for ions and protons. The peak right after the entry in a material, typical for the energy deposition caused by ions, can not be seen in Figure 14. The explanation is that the ion beam hits the pipe with a very

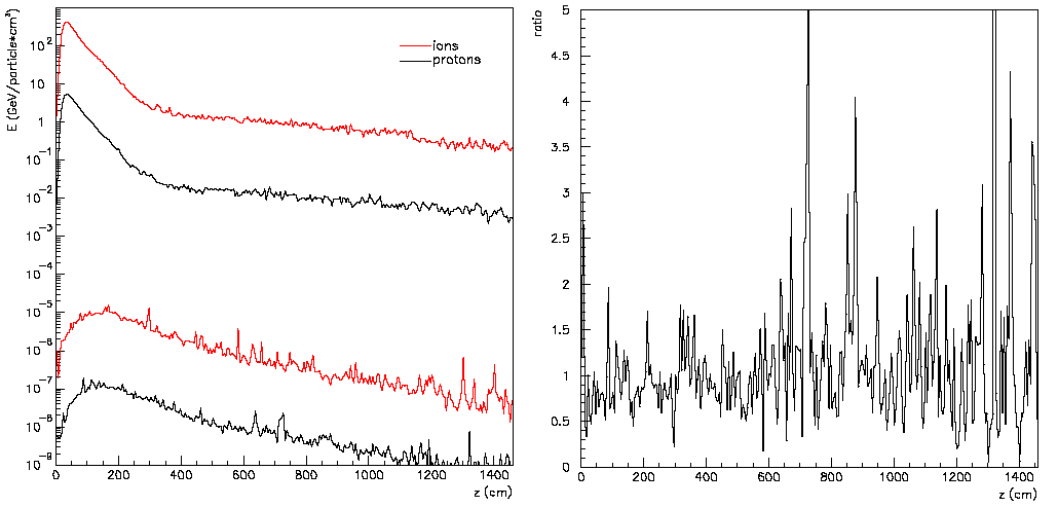

Figure 14: Left: The two upper curves show the energy deposition in the hottest part of the inner coil for ions and protons, and the two lower curves the energy deposition in the BLMs. Right: The ratio between ion and proton losses and signals as described by Equation (22).

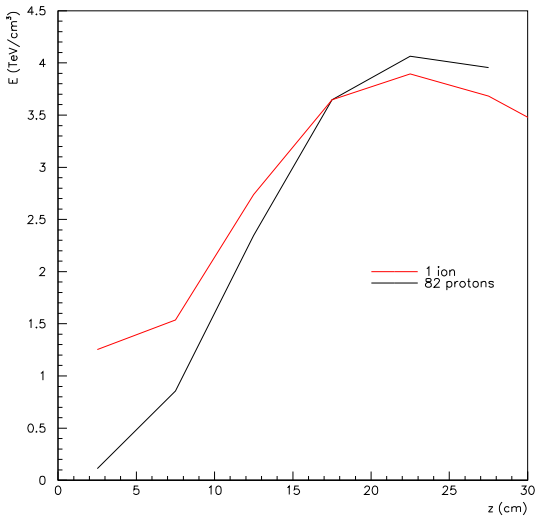

Figure 15: The energy deposition for one ion and 82 protons in the beam screen. In the very beginning, before the nuclear fragmentation, the energy deposited by the ion is higher due to the large cross sections for electromagnetic interactions.

small angle around 25 mrad. Therefore the first peak in the energy deposition is already in the beam screen and because of the angle it never reaches the coils. A new set of FLUKA simulations, where the energy deposition also in the beam screen was scored, confirms this. The result for both ions and protons is shown in Figure 15. The curve for protons was scaled with the energy ratio 2.76/7 between ions and protons and then multiplied with the number of nucleons, 208, in one lead ion in order to simplify the comparison. The resulting number of protons to compare with is 82.

So the conclusion of the simulation is that the lead ions and protons at LHC energies will have the same energy to signal ratio, meaning that the thresholds for the BLMs do not need to be changed. However, this conclusion is based also on the assumption that the losses for ions and protons occur in the same places around the LHC, since there is a certain spacing between the BLMs. For instance, at the spot where the lost ions from BFPP hit, there is no BLM placed in the present design. This means that the BLM catching the traces from BFPP will be too far away and therefore not make a correct estimation of the power deposition in the coil. Therefore, in order to safely operate the LHC, it is essential to place a BLM at this spot but also to investigate other sources of ion losses and determine the loss locations.

5 Conclusions

Beam losses due to Bound-Free Pair Production in lead-ion collisions may quench certain dipole magnets in the dispersion suppressors of the LHC. By means of tracking in the LHC optics and Monte-Carlo simulation of the shower in the superconducting magnet, we have evaluated the heat deposition that can be expected with the nominal peak luminosity $L = 1.0 \times 10^{27} \mathrm{cm}^{-2}\mathrm{s}^{-}1$ for colliding beams of $^{208}\mathrm{Pb}^{82+}$ of energy 0.574 PeV. The maximum of the radially-averaged power deposited in the coil was found to be approximately $7\,\mathrm{mW/cm^3}$.

In addition, we have made a revised evaluation of the levels of energy deposition, whether steady state or transient, that can lead to quenches of LHC dipole magnets. The acceptable level of steady-state losses appears to be substantially higher than previously supposed: the magnets should withstand a heating power of at least $10\,\mathrm{mW/cm^3}$ in steady state without quenching. Thus the secondary beam of ions emerging from each collision point is not likely to quench a dipole magnet. Although we must acknowledge that several uncertainties exist, this is an encouraging indication that the Bound-Free Pair Production in lead ion collisions will not be a practical limit to the luminosity of the LHC.

We have also evaluated the response of the LHC beam loss monitors to both proton and lead ion beam losses with the preliminary conclusion that similar quench thresholds can be used for both types of beam.

Of course, our estimates of the quench levels should be confirmed by further detailed calculations carried out by others.

6 Acknowledgements

The authors would like to thank the following persons for helpful information and discussions: Simona Bettoni, Alfredo Ferrari, Jean-Bernard Jeanneret, Daniel Leroy, Matteo Magistris, Stephan Russenschuck, Georg Smirnov and Davide Tommasini.

References

[1] O.S. Brüning, P. Collier, P. Lebrun, S. Myers, R. Ostojic, J. Pool, and J. Proudlock (editors). LHC design report v.1 : the LHC main ring. *CERN-2004-003-V1*, 2004.

[2] J. M. Jowett. Ions in the LHC ring. *Proceedings of the LHC Performance Workshop, Chamonix XII*, 2003.

[3] H. Meier et al. Bound-free electron-positron pair production in relativistic heavy-ion collisions. *Phys. Rev. A*, 63, 2001.

[4] S.R. Klein. Localized beam pipe heating due to e^- capture and nuclear excitation in heavy ion colliders. *Nuclear instruments and Methods in Physics Research A*, 459:51, 2001.

[5] H.F. Krause et al. Electron capture and ionization of Pb ions at 33 TeV. *Phys. Rev. Letters*, 80(6):51, 1998.

[6] S. Datz et al. Measurement of electromagnetic cross sections in heavy ion interactions and its consequences for luminosity lifetimes in ion colliders. *CERN SL-99-009*, 1999.

[7] J. M. Jowett, H.-H. Braun, M. I. Gresham, E. Mahner, A. N. Nicholson, E. N. Shaposhnikova, and I. A. Pshenichnov. Limits to the performance of LHC with ion beams. *proceedings of the 2004 European Particle Accelerator Conference, Lucerne, Switzerland*, page 578, 2004.

[8] A. Fasso et al. *Electron-photon transport in FLUKA: Status, invited talk in the Proceedings of the MonteCarlo 2000 Conference*, page 159. Springer-Verlag Berlin, 2001.

[9] A. Fasso et al. *FLUKA: Status and Prospective for Hadronic Applications, invited talk in the Proceedings of the MonteCarlo 2000 Conference*, page 955. Springer-Verlag Berlin, 2001.

[10] M. Magistris, private communication, 2004.

[11] S. Russenschuck, private communication, 2004.

[12] F. Sonnemann. *Resistive transition and protection of LHC superconducting cables and magnets*. PhD thesis, RWTH Aachen, 2001.

[13] C. Meuris et al. Heat transfer in electrical insulation of LHC cables cooled with superfluid helium. *Cryogenics*, 39:921, 1999.

[14] S. Eidelman et al. Review of Particle Physics. *Physics Letters B*, 592:1+, 2004.

[15] J.B. Jeanneret et al. Quench levels and transient beam losses in LHC magnets. *LHC Project Report 44*, 1996.

[16] J. H. Lienhard IV and J. H. Lienhard V. *A heat transfer textbook*. Phlogiston Press, 2003.

[17] M. Wilson. *Superconducting magnets*. Clarendon Press Oxford, 1983.

[18] D. Leroy, private communication, 2005.

[19] F. Sonnemann and M. Calvi. Quench simulation studies: Program documentation of SPQR Simulation Program for Quench Research. *LHC Project Note 265*, 2001.

[20] A. Siemko et al. Beam loss induced quench levels. *Proceedings of the LHC Performance Workshop, Chamonix XIV, CERN-AB-2005-014*, page 296, 2005.

[21] `http://www.users.uswest.net/~varp/hepak.htm`.

[22] J-B Jeanneret, private communication, 2005.

[23] `http://www.wolfram.com`.

[24] E. Gschwentdner et al. The beam loss detection system of the LHC ring. *CERN SL-2002-021*, 2002.

[25] E. B. Holzer et al. Design of the beam loss monitoring system for the LHC ring. *LHC Project Report 781*, 2004.